Rank Deficiency and Superstability of Hybrid Systems

Eric Wendel[a,*], Aaron D. Ames[a,2]

[a] *Texas A&M University, College Station, TX 77843*

Abstract

The objectives of this paper are to study the rank properties of flows of hybrid systems, show that they are fundamentally different from those of smooth dynamical systems, and to consider applications that emphasize the importance of these differences. It is well known that the flow of a smooth dynamical system has rank equal to the space on which it evolves. We prove that, in contrast, the rank of a solution to a hybrid system, a *hybrid execution*, is always less than the dimension of the space on which it evolves and in fact falls within possibly distinct upper and lower bounds that can be computed explicitly. The main contribution of this work is the derivation of conditions for when an execution fails to have maximal rank, *i.e.*, when it is rank deficient. Given the importance of periodic behavior in many hybrid systems applications, for example in bipedal robots, these conditions are applied to the special case of periodic hybrid executions. Finally, we use the rank deficiency conditions to derive *superstability* conditions describing when periodic executions have rank equal to 0, that is, we determine when the execution is completely insensitive to perturbations in initial conditions. The results of this paper are illustrated on three separate applications, two of which are models of bipedal walking robots: the classical single-domain planar compass biped and the two-domain planar kneed biped.

Keywords: Hybrid systems theory, Stability, Poincaré map, Bipedal robots

*Corresponding author. Graduate student, Aerospace Engineering.
Email addresses: ericdbw@tamu.edu (Eric Wendel), aames@tamu.edu (Aaron D. Ames)
[1] Assistant Professor, Mechanical Engineering.
[2] This research is supported in part by NSF award CNS-0953823 and NHARP Award 000512-0184-2009.

1. Introduction

Hybrid systems consist of both continuous and discrete components and, as such, are capable of modeling a wide variety of physical systems, *i.e.*, systems that evolve with both continuous and discrete dynamics. Applications that exhibit hybrid dynamics include embedded computer systems, in which digital circuits control continuous physical processes, and multi-modal, multi-agent systems, such as vehicle and air transportation systems [1, 2]. The hybrid systems framework also subsumes [3] models of systems with discontinuous changes in state, for example those subject to complementarity conditions [4] or modeled with differential inclusions [5].

Although hybrid systems model a wide variety of applications, we may not in general assume that hybrid systems share the same fundamental properties as smooth dynamical systems. Moreover, the interaction of the smooth and discrete components of a hybrid system can result in solution behavior that is impossible for smooth dynamical systems to exhibit. For example, the existence and uniqueness properties of solutions of hybrid systems — called *hybrid executions* — are not the same as for smooth systems [6, 7]; therefore, one may not regard the stability of hybrid system equilibria in the same way as the stability of smooth system equilibria [8]. An example of the fundamental difference between the solutions of smooth and hybrid systems is *Zeno behavior*, where under certain conditions an execution of a hybrid system can take an infinite number of discrete transitions in a finite amount of time [9].

Recent work has also shown that Poincaré maps for hybrid systems are fundamentally different from Poincaré maps for smooth systems. Recall from the standard theory of smooth dynamical systems that the linearization of the flow at a point in a closed and periodic orbit will always have one eigenvalue equal to 1. This property has never been observed for linearizations of the executions of hybrid systems; in [10] it was observed that finite difference approximations of the linearization of the execution always have one eigenvalue equal to 0, but the lack of agreement with the standard theory was not explained. On the other hand in [11] and in [12, 13] the eigenvalue equal to 1 is recovered through formulae that are not always well-defined for arbitrary hybrid systems. Motivated by applications to bipedal robotics, the authors proved in [14] that these discrepancies in the literature are in fact due to fundamental differences in the rank

properties of Poincaré maps for smooth and for hybrid systems.

The first contribution of the present work is the extension of the results in [14] to arbitrary, non-periodic hybrid executions. In particular, we show that the rank of an execution will always fall between possibly distinct upper and lower bounds, and that the upper bound is always less than the dimension of the space on which the execution evolves. This result is in marked contrast with smooth dynamical systems, where the rank of a solution is strictly equal to the dimension of the space. Our primary contribution, however, is the derivation of conditions describing when an execution fails to have maximal rank, that is, when it is *rank deficient*. The main result shows that rank deficiency is caused by the alignment of the tangent space over the execution with the nullspace of each reset map. Since the reset maps of a hybrid system describe the transitions between the discrete components, the main result reinforces the fact that hybrid systems are fundamentally different objects from smooth systems.

The secondary contribution of this work emerges from application of the main result to periodic solutions of hybrid systems. We show that when an execution is periodic *and* rank deficient it may be possible for the system to be *superstable*. Recall that a discrete dynamical system is said to be superstable when it is completely insensitive to perturbations in initial conditions [15]. This occurs when the linearization of the discrete dynamical system is equal to 0 at a superstable equilibrium point. By considering superstability from within the context of rank deficiency of executions, we obtain a condition describing when a periodic hybrid execution is completely insensitive to perturbations in its initial conditions.

The application of the results of this paper to periodic systems is motivated by examples from the area of bipedal robotics. Bipedal locomotion consists of a "swing" phase followed by a discrete impact of the biped's foot with the ground, so a biped robot is naturally a hybrid system. A stable walking gait is therefore a stable periodic hybrid execution. McGeer's groundbreaking results [16] revealed that uncontrolled planar bipeds walking down shallow slopes have stable, human-like walking gaits. The rich *passive dynamics* of these walking gaits were thoroughly examined by Goswami *et. al.* [10] and exploited with great success in the construction of a 3D passive biped that was unfortunately not robust to perturbations in initial conditions [17].

We foresee that the superstability conditions presented here could enable the design of controllers that reduce our systems' sensitivity to perturbations. In [18], finite-time controllers and the properties of feedback-linearized systems are used to reduce the stability analysis of a planar biped to an interval of the real line. We foresee that, in analogy to this work, our rank deficiency conditions could be used to enable the design of (feedback-linearizing) controllers that reduce the stability analysis of complex 3D bipedal systems to lower-dimensional spaces by designing virtual constraints based upon these rank deficiency conditions. That is, obtaining controllers that result in rank deficiency would result in additional stability in the system, due to the connection between rank deficiency and superstability. So, by exploiting the fundamental differences between dynamic and hybrid systems, controllers could be designed that could increase the stability of systems modeled as hybrid systems.

Finally, it is worth noting that, to the authors' knowledge, there is no prior literature that directly addresses the fundamental rank properties of hybrid executions, nor the implications of rank deficiency to the periodic stability of hybrid systems.

We begin our analysis with a review of the standard theory of smooth dynamical systems in Section 2. We show that the continuous-time flow of a smooth vector field can be viewed as a discrete map [19, 20]. This standard theory applies directly to the smooth components of a hybrid system, leading to straightforward techniques for linearizing executions of hybrid systems, in Section 3. Using the linearization of a hybrid system we determine the rank of arbitrary hybrid executions and derive necessary and sufficient conditions for the rank of an execution to fall below its upper bound. These are the rank deficiency conditions. In Section 4 we specialize the rank deficiency conditions to periodic hybrid systems and their executions, called hybrid periodic orbits. A necessary and sufficient condition for a hybrid periodic orbit to be superstable is illustrated on a 2-domain hybrid system. The rank deficiency and superstability properties are illustrated on two separate examples of a planar bipedal robot. In the first, we show that the linearization of the hybrid periodic orbit of a 2-link planar compass biped accurately detects the occurrence of a period-doubling bifurcation. In the second, we show that although a planar kneed biped is capable of superstability, our particular limit cycle is not even rank deficient.

2. Smooth dynamical systems

In this section we review standard results [19] on the trajectories of smooth dynamical systems that will be necessary to our analysis of hybrid systems in Section 3. In particular we review how the flow, which depends continuously on time, can be viewed as a discrete map. When the flow is a closed and periodic orbit this perspective results in the well-known results on periodic stability of smooth dynamical systems [20]. As we will see in the following section, these standard results apply to hybrid systems since a hybrid system consists of collections of smooth and discrete components, and the smooth components are the integral curves to smooth vector fields.

A smooth dynamical system is a tuple (M, f), where M is a smooth manifold with tangent bundle TM and $f : M \to TM$ is a smooth vector field such that for the canonical projection map $\pi : TM \to M$, $\pi \circ f = \mathrm{Id}$, where Id is identity on M. We will assume that $M \subset \mathbb{R}^n$, in which case we can write the vector field in coordinates as $\dot{x} = f(x)$ with $x \in M \subset \mathbb{R}^n$ where necessarily $\dot{x} \in T_x M$. A smooth function $g : M \to N$ between manifolds induces a map between the tangent space $Dg(x) : T_x M \to T_{g(x)} N$; this is just the Jacobian or derivative.

2.1. Flows and variational equations

The unique solution to the differential equation $\dot{x} = f(x)$ with initial condition $x_0 \in M$ is a trajectory $c : I \subset [0, \infty) \to M$ such that $c(t_0) = x_0$ if $I = [t_0, t_1]$, for some $t_1 > t_0$. We refer to this curve as an *integral curve* or *orbit* of $f(x)$. The *flow* of the smooth vector field $\dot{x} = f(x)$ is a smooth map $\phi : I \times U \to U' \subset M$, where U is some neighborhood of $x_0 = c(t_0)$, satisfying the following properties for all $r, s, t \in I$,

$$\begin{aligned} c(t_0) &= \phi_0(c(t_0)) \\ c(t_0 + t + s) &= \phi_{t+s}(c(t_0)) = \phi_t \circ \phi_s(c(t_0)) \\ \phi_{-r} \circ \phi_r(x_0) = x_0 &\Rightarrow \phi_{-r} = (\phi_r)^{-1} \end{aligned}$$

The flow, with t considered a parameter, is a diffeomorphism $\phi_t : U \to U'$, for all $t \in I$.

The *space derivative* of $\phi_t(x_0)$ is simply the partial derivative of the flow with respect to its second argument,

$$D_x \phi_t(x_0) := \frac{\partial \phi_t(x_0)}{\partial x_0}.$$

The space derivative is also the so-called fundamental matrix solution to the *variational equation* [19, 21, 20]. The variational equation is the nonautonomous linear differential equation

$$\dot{z}(t) = A(t)\, z(t) \tag{1}$$

obtained by linearizing the vector field f along the flow with initial condition x_0, where $A(t) := Df\big(\phi_t(x_0)\big)$ and $z(t) := \dot{\phi}_t(x_0)$. Associated with this linear system is the *fundamental matrix equation*

$$\dot{\Phi}(t) = A(t)\, \Phi(t), \tag{2}$$

with solution $\Phi(t) = D_x\phi_t(x_0)$. As an integral curve, $\Phi(t)$ is nonsingular for all t and has the property that

$$\dot{\phi}_t(x_0) = \Phi(t)\Phi^{-1}(0)\, \dot{\phi}_0(x_0) = \Phi(t)\, \dot{\phi}_0(x_0).$$

That is, with $x_1 = \phi_t(x_0)$,

$$\begin{aligned} \dot{\phi}_t(x_0) &= \Phi(t)\, \dot{\phi}_0(x_0), \\ f(x_1) &= \Phi(t)\, f(x_0). \end{aligned} \tag{3}$$

Note in particular that $\Phi(0) = \mathrm{Id}_n$, the $n \times n$ identity matrix.

If an expression for the flow is known in closed form then $\Phi(t)$ can be obtained by directly computing partial derivatives. Otherwise, the flow and its fundamental matrix must be obtained by simultaneous numerical integration, as described in [21, 22]. As we will see in the following Sections, accurate computation of the fundamental matrix is an important issue, as it plays an important role in assessing periodic stability.

2.2. Flows to sections

In this Section we determine the properties of flows that reach, or intersect with, a certain smooth hypersurface called a *local section*. Historically, analysis of flows to local sections has been restricted to the special case of closed orbits [19, 20], which we review in Section 2.4. However, as we will see in Section 3, since solutions of a hybrid system consist entirely of flows that are permitted to evolve only until they reach a local section, the properties of flows to sections are most pertinent to the analysis of hybrid systems.

Definition 1. A *local section* of a vector field $\dot{x} = f(x)$ on M is a smooth codimension-1 submanifold S of M that is also *transverse* to the flow.

$$S = \{x \in M \mid h(x) = 0 \text{ and } L_f h(x) \neq 0\},$$

where $h : M \to \mathbb{R}$ is a C^1 function and $L_f h$ is the Lie derivative. More generally, any submanifold $N \subset M$ is said to be *transverse* to the flow (or vector field f) if $f(x)$ is not in $T_x N$.

It is possible to construct a local section through any point of the flow that is not an equilibrium point [23].

Lemma 1 (Smale, 1963)**.** *Let $f(x)$ be a vector field defined on a smooth manifold M. If $f(x) \neq 0$ for some $x \in M$ then there exists a local section S through x.*

The time it takes a flow to reach a local section is given by a well-defined map. We reproduce the following Lemma from [19], the proof of which follows from direct application of the implicit function theorem.

Lemma 2 (Hirsch & Smale, 1974)**.** *Let S be a local section, $x_0 \in M$ and $x_1 = \phi_t(x_0) \in S$. There exists a unique, C^1 function $\tau : U_0 \to [0, \infty)$ called the time-to-impact map such that for U_0 a sufficiently small neighborhood of x_0, $\phi_{\tau(x)}(x) \in S$ for all $x \in U_0$.*

The Lemma allows us to view the flow to a section as a discrete map $\phi_\tau : U_0 \to V$ defined by $\phi_\tau(x) := \phi_{\tau(x)}(x)$ for all $x \in U_0$, where U_0 is defined as above and $V := \phi_\tau(U_0) \cap S$ is the image of ϕ_τ in S.

It is important to realize that the map ϕ_τ does not have the same properties as the flow, ϕ_t. In particular, the map ϕ_τ depends implicitly on, and is an implicit function of, the local section S, whereas ϕ_t does not depend implicitly or explicitly on S. In the next subsection we review an important consequence of this fact: that ϕ_τ does not have the same rank as the flow.

2.3. Rank of flows to sections

The flow $\phi_t : U \to U'$, with t considered a fixed parameter, is a diffeomorphism, so its total derivative, $D\phi_t$, will always have full rank. This is easily confirmed by computing

$$D\phi_t(x) = D_x \phi_t(x) = \Phi(t),$$

which is nonsingular.

We likewise determine the rank of $\phi_\tau : U_0 \to V \subset S$ by computing the rank of its derivative, or linearization, at some point $x_0 \in U_0$:

$$\begin{aligned} D\phi_\tau(x_0) &= \Phi(\tau(x_0)) + \dot{\phi}_\tau(x_0) D\tau(x_0) \\ &= \left(\mathrm{Id}_n - \frac{f(x_1)Dh(x_1)}{L_f h(x_1)} \right) \Phi(\tau(x_0)), \end{aligned} \tag{4}$$

where $x_1 = \phi_\tau(x_0)$ and Id_n is the $n \times n$ identity matrix. The derivative of the time-to-impact map was obtained from the proof of Lemma 2 in [19],

$$D\tau(x_0) = -\frac{Dh(x_1)\Phi(\tau(x_0))}{L_f h(x_1)}, \tag{5}$$

where h defines the section S, as in Definition 1. The following Theorem from [14] shows that equation (4) has a nullspace and, as we will see, prevents the extension of theorems on closed orbits to periodic executions of hybrid systems.

Theorem 3. *Let S be a local section and $x_0 \in U_0$ with S and U_0 as in Lemma 2. If $\dim(M) = n$ then $D\phi_\tau(x_0)$ has rank $n-1$ if and only if $x(t) = \phi_t(x_0)$ is not a closed orbit. Moreover, the nullspace is*

$$\mathrm{ns}(D\phi_\tau(x_0)) = \mathrm{span}\{f(x_0)\}. \tag{6}$$

In general, the flow to a section has rank equal to the dimension of the section and so the total derivative of a non-closed flow to a section is a only diffeomorphism between local sections. A proof of the following result is also in [14].

Corollary 4. *Let $x_0 \in M$ with S_0 a local section through x_0, S a local section through $x_1 = \phi_t(x_0)$ and U_0 a neighborhood of x_0 such that $\phi_\tau(x) \in S$ for all $x \in U_0$. Then for $V_0 := U_0 \cap S_0$ and $V := \phi_\tau(U_0) \cap S$, the restriction map $\phi_\tau : V_0 \to V$ is a diffeomorphism.*

Using the Lemmas and Theorems discussed thus far we may summarize the standard properties of flows to sections as follows:

(**S1**) Lemma 1 implies that for a local section S of $c(t_0)$ there exists a sufficiently small neighborhood U_0 of $c(t_0)$ such that $\phi_\tau(U_0) \subset S$.

(**S2**) From Theorem 3 and Corollary 4 we know there exists a local section S_0 through $c(t_0)$ such that for $V_0 := U_0 \cap S_0$ and $V := \phi_\tau(U_0) \cap S$, the restricted map $\phi_\tau : V_0 \to V$ is a diffeomorphism with rank $n-1$.

These properties are generically satisfied by flows to sections, and will be revisited when we discuss hybrid systems in Section 3.

2.4. Closed orbits

It is well-known [19, 20] that the stability of a closed orbit is equivalent to the stability of the Poincaré map associated with it. Let x^* be the initial condition of the flow and define a local section S through x^*. If the flow intercepts S at least once more then we may define the *first-return map* $\phi_\tau : U_0 \to S$, such that $x^* = \phi_\tau(x^*)$, with U_0 defined as in Lemma 2. Using equation (3) it is easy to see, with $x_0 = x^* = \phi_\tau(x^*) = x_1$, that

$$f(x^*) = \Phi(\tau(x^*))\, f(x^*).$$

In other words, the space derivative of the closed orbit has an eigenvalue equal to 1 with eigenvector $f(x^*)$.

Since all points of $V_0 := U_0 \cap S$ also reach S, the *Poincaré map* of the closed orbit is the restriction of the first-return map $P = \phi_\tau|_{V_0} : V_0 \to S$. The Poincaré map is thus a discrete dynamical system with fixed point $x^* = P(x^*)$. As the restriction map, the Poincaré map necessarily has rank $n-1$ and, as a consequence, the stability of a Poincaré map is determined by its $n-1$ eigenvalues being within the unit circle. The following result due to [20] relates the total and space derivatives of the periodic flow to the total derivative of the Poincaré map.

Theorem 5 (Perko)**.** *The total derivative of the Poincaré map $P = \phi_\tau|_{V_0} : V_0 \to S$ at x^* depends only on the space derivative at $x^* = \phi_\tau(x^*)$. That is,*

$$D\phi_\tau(x^*) = \Phi(\tau(x^*)).$$

Since $\Phi(\tau(x^*))$ has an eigenvalue equal to 1 with eigenvector

$$f(x^*) = \Phi(\tau(x^*))f(x^*),$$

when coordinates on M are chosen so that $f(x^*) = (0, \ldots, 1)^T$ then

$$\tilde{\Phi} = DP(x^*)$$

where $\tilde{\Phi}$ is the first $n-1$ rows and $n-1$ columns of $\Phi(\tau(x^*))$ in the chosen coordinates. Thus $P(x^*)$ is exponentially stable if and only if the $n-1$ eigenvalues of $\tilde{\Phi}$ are within the unit circle.

Remark 1. Theorem 5 states that the total derivative of the flow at $x^* = \phi_\tau(x_0) = x^*$ has full rank n if and only if it is a closed orbit. However, Theorem 3 states that the nullspace of the total derivative of the flow at $x^* = \phi_\tau(x_0)$ is spanned by $f(x_0)$ if and only if it is not closed, that is if $x^* \neq x_0$. To summarize, the main difference between a closed and a non-closed orbit is that

$$D\phi_\tau(x_0)\, f(x_0) = \begin{cases} f(x_0), & \text{if } x^* = \phi_\tau(x_0) = x_0, \\ 0, & \text{if } x^* = \phi_\tau(x_0) \neq x_0. \end{cases}$$

In the periodic case we have that $f(x_0) = f(x^*)$ is an eigenvector of the total derivative of the flow to the section with eigenvalue equal to 1. In the non-closed case, instead of being an eigenvector, $f(x_0)$ spans the total derivative's nullspace.

As we will see in the following Section, solutions of a hybrid system consist, by definition, of non-closed orbits. Thus, an important consequence of these properties is that periodic solutions of hybrid systems cannot possibly have the eigenvalue properties of a closed orbit. Any claims to the contrary would need to show that $f(x_0)$ is an eigenvector of the linearization of an execution with eigenvalue equal to 1, but this is definitively ruled out by the properties just mentioned. In fact, Theorem 3 leads directly to the rank properties that we derive in the following Sections, cf. Lemma 7. See [14] for more details on the fundamental differences between the periodic stability of smooth and hybrid systems. Our study of the mechanisms causing rank deficiency in arbitrary hybrid executions is motivated by these fundamental differences.

3. Hybrid dynamical systems

Our objective is to understand the rank properties of arbitrary hybrid executions in order to enable the design of controllers that improve the stability properties of hybrid systems. To this end, we use basic linear algebra to derive the conditions under which rank deficiency occurs and then discuss how these conditions can be used in controller design.

3.1. Hybrid systems and executions

We begin by revisiting the results of the previous section from the perspective of hybrid systems and their executions.

Definition 2. A hybrid system is a tuple

$$\mathcal{H} = (\Gamma, D, G, R, F)$$

where

- $\Gamma = (Q, E)$ is a graph such that $Q = \{q_1, \ldots, q_k\}$ is a set of k vertices and $E = \{e_1 = (q_1, q_2), e_2 = (q_2, q_3), \ldots\} \subset Q \times Q$. With the set E we define maps sor : $E \to Q$ which returns the source of an edge, the first element in the edge tuple, and tar : $E \to Q$, which returns the target of an edge or the second element in the edge tuple.
- $D = \{D_q\}_{q \in Q}$ is a collection of smooth manifolds called *domains*, where D_q is assumed to be an embedded submanifold of $\mathbb{R}^{n_q}$ with $\dim(D_q) = n_q \geq 1$.
- $G = \{G_e\}_{e \in E}$ is a collection of *guards*, where G_e is assumed to be an embedded submanifold of $D_{\mathrm{sor}(e)}$.
- $R = \{R_e\}$ is a collection of *reset maps* which are smooth maps $R_e : G_e \to D_{\mathrm{tar}(e)}$.
- $F = \{f_q\}_{q \in Q}$ is a collection of Lipschitz vector fields on D_q, such that $\dot{x} = f_q(x)$.

The continuous and discrete dynamics of a hybrid system are described using a notion of solution called a hybrid execution. Where a smooth dynamical system is said to generate solutions, a hybrid system is said to *accept* an execution; see [6] for more background on solutions of hybrid systems.

Definition 3. A *hybrid execution* is a tuple

$$\chi = (\Lambda, I, \rho, C)$$

where

- $\Lambda = \{0, 1, 2, 3, \ldots\} \subseteq \mathbb{N}$ is a finite or infinite indexing set.
- $I = \{I_i\}_{i \in \Lambda}$ such that with $|\Lambda| = N$, $I_i = [t_i, t_{i+1}] \subset \mathbb{R}$ and $t_i \leq t_{i+1}$ for $0 \leq i < N - 1$. If N is finite then $I_{N-1} = [t_{N-1}, t_N]$ or $[t_{N-1}, t_N)$ or $[t_{N-1}, \infty)$, with $t_{N-1} \leq t_N$.

- $\rho : \Lambda \to Q$ is a map such that $e_{\rho(i)} := (\rho(i), \rho(i+1)) \in E$.
- $C = \{c_i\}_{i \in \Lambda}$ is a set of continuous trajectories where each c_i is the integral curve of the vector field $f_{\rho(i)}$ on $D_{\rho(i)}$. Specifically, $c_i(t) = \phi^{\rho(i)}_{t-t_i}(c_i(t_i))$, where $\phi^{\rho(i)}_t$ is the flow associated with $f_{\rho(i)}$.

We require the consistency conditions:

- For $i < |\Lambda|$ and for all $t \in I_i$,

$$c_i(t) \in D_{\rho(i)} \text{ and } c_i(t_{i+1}) \in G_{e_{\rho(i)}},$$
$$c_i(t_i) = \phi^i_0(c_i(t_i)).$$

- For $i < |\Lambda| - 1$,

$$R_{e_{\rho(i)}}(c_i(t_{i+1})) = c_{i+1}(t_{i+1}).$$

3.1.1. Assumptions

We will only consider hybrid executions that are *deterministic* and *non-blocking* [6]. We further impose the following conditions on χ in order to ensure that the guards and reset maps are sufficiently "well-behaved." Let $i < |\Lambda| - 1$ and $e = (\rho(i), \rho(i+1))$.

(A1) The execution does not have any equilibria, *i.e.*, $f_{\rho(i)}(c_i(t)) \neq 0$, for all $t \in I_i$.

(A2) R_e has constant rank r_e and $R_e(G_e)$ is a submanifold of $D_{\mathrm{tar}(e)}$.

(A3) G_e is a section, *i.e.*, $\dim(G_e) = \dim(D_{\mathrm{sor}(e)}) - 1$ and $f_{\mathrm{sor}(e)}(x) \notin T_x G_e$ for all $x \in G_e$. Furthermore, there exist subsets $S^i \subset G_e$ that are also local sections.

(A4) $R_e(G_e)$ is transverse to $f_{\mathrm{tar}(e)}$ whenever $\dim(D_{\mathrm{sor}(e)}) \leq \dim(D_{\mathrm{tar}(e)})$, that is, when $f_{\mathrm{tar}(e)}(y) \notin T_y R_e(G_e)$ for all $y \in R_e(G_e)$.

Remark 2. The final condition (**A4**) asserts that the target vector field is not tangent to the image of the reset map whenever the reset maps to a larger-dimensional domain. This is a reasonable assumption to make, since if $\dim(D_{\mathrm{sor}(e)}) \leq \dim(D_{\mathrm{tar}(e)})$ then the maximum dimension of the submersed submanifold $R_e(G_e)$ is

$$\max(\dim(R_e(G_e))) = \dim(D_{\mathrm{sor}(e)}) - 1 < \dim(D_{\mathrm{tar}(e)}),$$

implying that it is possible for $R_e(G_e)$ to be a codimension-m local section, where $m = \dim(D_{\text{tar}(e)}) - \dim(D_{\text{sor}(e)}) + 1$.

The converse is a much stronger assumption, so we do not make it; we do not assume that $R_e(G_e)$ is a local section when $\dim(D_{\text{sor}(e)}) > \dim(D_{\text{tar}(e)})$ because it is possible that if $\dim(R_e(G_e)) = \dim(D_{\text{tar}(e)})$ then $f_{\text{tar}(e)}(y) \in T_y R_e(G_e)$ for all $y \in R_e(G_e)$.

As we will see, this transversality condition on $R_e(G_e)$ will allow us to tighten the lower bound on the rank of our executions.

3.1.2. Properties

We may extend properties (**S1-2**) of flows to sections from Section 2 to every integral curve $c_i \in C$, $i < |\Lambda|$, satisfying (**A1-4**). These properties are generically satisfied by any flow that reaches a guard, and will be necessary to our results on rank deficiency in the following subsections.

(H1) Lemma 1 implies that for a local section $S^i \subset G_e$ of $c_i(t_{i+1})$ there exists a sufficiently small neighborhood U_0^i of $c_i(t_i)$ such that $\phi_\tau^{\rho(i)}(U_0^i) \subset S^i$.

(H2) From Theorem 3 and Corollary 4 we know there exists a local section S_0^i through $c_i(t_i)$ such that for $V_0^i := U_0^i \cap S_0^i$ and $V^i := \phi_\tau^{\rho(i)}(U_0^i) \cap S^i$, the restricted map $\phi_\tau^{\rho(i)} : V_0^i \to V^i$ is a diffeomorphism with rank equal to $\dim(D_{\rho(i)}) - 1$.

Remark 3. It is easy to see that properties (**S1-2**) of flows to sections do indeed extend naturally to the integral curves of a hybrid execution. Note that transverse coincidence of an integral curve with a local section of a guard triggers a discrete transition to the next or the same domain in the hybrid system graph. This means that the integral curves of an execution are not permitted to evolve past local sections; they are implicit functions of the local sections.

It is of course possible to conceive of examples of hybrid systems where the flow reaches a guard but does not trigger a discrete transition. Such hybrid systems are called *trivial*. The reset maps of a trivial hybrid system are necessarily equal to identity and likewise the vector fields are all the same, $f_q = f$ for all $q \in Q$, so that the hybrid execution χ can be written as the continuous flow of a single vector field. For such systems, the integral curves are not implicit functions of the local sections and so the

properties of flows to sections cannot be extended to them. Such systems should be analyzed as smooth dynamical systems. We henceforth consider only non-trivial hybrid systems.

3.1.3. Fundamental hybrid executions

The rank of a hybrid execution is determined by the rank of its linearization, or total derivative, at every point. This motivates the following definition.

Definition 4. The *fundamental hybrid execution* associated with a given execution χ is a tuple

$$\mathcal{F}\chi = (\Lambda, I, \rho, C, W)$$

where Λ, I, ρ, and C are given in Definition 3 and $W = \{\Phi_i\}_{i\in\Lambda}$ is a set of continuous matrix-valued trajectories. Here each Φ_i is the integral curve of the vector field $\dot{\Phi}_i(t - t_i) = Df_{\rho(i)}(c_i(t))\,\Phi_i(t - t_i)$. Specifically, $\Phi_i(t - t_i) = D_x\phi^{\rho(i)}_{t-t_i}(c_i(t_i))$; that is, each $\Phi_i \in W$ is the fundamental matrix or space derivative of the flow evaluated along the integral curve $c_i \in C$. In addition, for $i < |\Lambda|$ and for all $t \in I_i$, we require the consistency condition:

$$\dot{\phi}^i_t(c_i(t_i)) = \Phi_i(t - t_i)\,\dot{\phi}^i_0(c_i(t_i)).$$

As mentioned in Section 2, if numerical computation is necessary, the vector field $f_{\rho(i)}$ and fundamental matrix equation $\dot{\Phi}_i$ must be integrated simultaneously. In the next subsection we show how to use $\mathcal{F}\chi$ to obtain the rank of χ, and thereafter it will be assumed that $\mathcal{F}\chi$ is available whenever it is necessary to compute the total derivative of the flow on a domain.

3.2. Rank of hybrid executions

Let $\mathcal{H}$ be a hybrid system and χ its hybrid execution with initial condition in the guard, $c_0(t_0) \in G_{e_{\rho(0)}}$. We are interested in finding a function relating the initial condition to a point $c_i(t_{i+1})$ in the guard $G_{e_{\rho(i)}}$, for some $i < |\Lambda|$. In fact this relation is given by the *partial* function $\psi_{\rho(i)} : V^0 \to V^i$ defined by $c_i(t_{i+1}) = \psi_{\rho(i)}(c_0(t_0))$, with

$$\psi_{\rho(i)} = \phi^{\rho(i)}_\tau \circ R_{e_{\rho(i-1)}} \circ \cdots \circ \phi^{\rho(1)}_\tau \circ R_{e_{\rho(0)}}, \tag{7}$$

and the neighborhoods V^0 and V^i of $c_0(t_0)$ and $c_i(t_{i+1})$ defined as in (**H2**). We may think of the partial function as describing the progress of the execution through the hybrid system $\mathcal{H}$.

Remark 4. This sequence of discrete maps $\psi_{\rho(i)}$ is a partial function since there is no guarantee that all of the points in the image of each reset map reach the guard. More precisely, we could call $\psi_{\rho(i)}$ a function if we could guarantee that $R_{e_{\rho(j)}}(\phi_\tau^{\rho(j)}(U_0^j)) \subset U_0^{j+1}$ for every $j \leq i-1 < |\Lambda|$. This condition can be met if each neighborhood U_0^j is made sufficiently small.

Let $\mathcal{F}\chi$ be the fundamental execution associated with χ. The total derivative of (7) is

$$D\psi_{\rho(i)} = D\phi_\tau^{\rho(i)} \circ DR_{e_{\rho(i-1)}} \circ \cdots \circ D\phi_\tau^{\rho(1)} \circ DR_{e_{\rho(0)}}, \tag{8}$$

where for all $j \leq i$, $DR_{e_{\rho(j)}}$ is the Jacobian of $R_{e_{\rho(j)}}$. We compute $D\phi_\tau^{\rho(j)}$ using (4) and the matrices $\Phi_i \in W$ of the fundamental execution associated with χ, as follows. For ease of notation let $x_0 = c_j(t_j)$, $x_1 = c_j(t_{j+1})$ and $h_j : D_{\rho(j)} \to \mathbb{R}$ define the local section $S^j \subset G_{e_{\rho(j)}}$ as in Definition 1. Then,

$$\begin{aligned} D\phi_\tau^{\rho(j)}(x_0) &= \Phi_j(\tau(x_0)) + f_{\rho(j)}(x_0)\, D\tau(x_0) \\ &= \left(\mathrm{Id}_{n_j} - \frac{f_{\rho(j)}(x_1)\, Dh_j(x_1)}{Dh_j(x_1)\, f_{\rho(j)}(x_1)}\right) \Phi_j(\tau(x_0)), \end{aligned} \tag{9}$$

where $\tau(x_0) = t_{j+1} - t_j$ is the time it takes the flow to reach the guard and $n_j = \dim(D_{\rho(j)})$ is the dimension of the manifold. For the sake of convenience, in the following discussion we will not explicitly use $\mathcal{F}\chi$, and will merely assume that the fundamental execution is available whenever it is necessary to compute $D\phi_\tau^{\rho(j)}$.

Our analysis of the rank properties of χ is aided by identifying the terms in equation (7) that can be associated with each edge in the graph Γ of $\mathcal{H}$.

Definition 5. Let $i < |\Lambda| - 1$. For every edge $e = (\rho(i), \rho(i+1)) \in E$, the *edge map* $\psi_e : V^i \to V^{i+1}$ takes the guard of one domain to the next and is defined by

$$\psi_e = \phi_\tau^{\mathrm{tar}(e)} \circ R_e.$$

We use the edge map to rewrite equations (7) and (8) as

$$\psi_{\rho(i)} = \psi_{e_{\rho(i-1)}} \circ \cdots \circ \psi_{e_{\rho(0)}}, \tag{10}$$

$$D\psi_{\rho(i)} = D\psi_{e_{\rho(i-1)}} \circ \cdots \circ D\psi_{e_{\rho(0)}}. \tag{11}$$

It is now necessary to recall some basic facts from linear algebra in order to prove our rank deficiency conditions. First, we recall that the rank of the composition of linear maps falls between possibly distinct upper and lower bounds. Let $\{A_i\}_{i=1}^k$ be a collection of $n_{i+1} \times n_i$ real-valued matrices. It can easily be shown using repeated application of Sylvester's inequality that the rank of their composition, $\prod_{i=1}^k A_i = A_1 \circ A_2 \circ \cdots \circ A_k$, is bounded above and below by

$$\operatorname{rank}\left(\prod_{i=1}^{k} A_i\right) \leq \min_{i\in\{1,\ldots,k\}} \{\operatorname{rank}(A_i)\}, \tag{12}$$

$$\operatorname{rank}\left(\prod_{i=1}^{k} A_i\right) \geq \sum_{i=1}^{k} \operatorname{rank}(A_i) - \sum_{i=1}^{k-1} n_i. \tag{13}$$

We will also make use of the rank-nullity theorem [24] from linear algebra: for a linear map $A : \mathbb{R}^n \to \mathbb{R}^m$,

$$\operatorname{rank}(A) + \operatorname{nty}(A) = n,$$

where $\operatorname{nty}(A)$ is the dimension of the nullspace of A. Finally, we use rank-nullity and [24] to prove the following basic Lemma on the nullity of the composition of linear maps.

Lemma 6. *Let A and B be linear maps. Then*

$$\operatorname{nty}(B \circ A) - \operatorname{nty}(A) = \dim(\operatorname{ns}(B) \cap \operatorname{im}(A)).$$

Proof. Let $\alpha = \{a_1, \ldots, a_r\}$ be a basis for $\operatorname{ns}(A)$ and $\beta = \{b_1, \ldots, b_q\}$ a basis for $\operatorname{ns}(B) \cap \operatorname{im}(A)$. By the rank-nullity theorem $r + q \leq n$. Let $\{a_{r+1}, \ldots, a_{r+q}\}$ be the elements of $\mathbb{R}^n$ that A maps to the basis β, such that $b_i = A(a_{r+i})$ for all $i \in \{1, \ldots, q\}$. It suffices to show that $\{a_1, \ldots, a_r, a_{r+1}, \ldots, a_{r+q}\}$ is a basis for $\operatorname{ns}(B \circ A) \subseteq \mathbb{R}^n$.

Note that since $\{a_{r+i}\}_{i=1}^q$ maps to a basis the set must be linearly independent. It follows that since $\{a_i\}_{i=1}^r$ is also a basis, $\{a_i\}_{i=1}^{r+q}$ must be linearly independent. To see this, realize that since $\{a_i\}_{i=1}^r$ is also a basis, $\{a_i\}_{i=1}^{r+q}$ is linearly dependent if and only if

$$\sum_{i=1}^{r} x_i a_i = -\sum_{j=1}^{q} y_j a_{r+j}$$

for arbitrary numbers $x_1, \ldots, x_r$ and $y_1, \ldots, y_q$. But this would imply that the nullspace of A is the linear combination of elements in the basis of the image of A, which is impossible. Hence,

$$\begin{aligned} r + q &= \dim(\mathrm{ns}(A)) + \dim(\mathrm{ns}(B) \cap \mathrm{im}(A)) \\ &= \dim(\mathrm{ns}(B \circ A)), \end{aligned}$$

proving our claim. □

The above Lemma and the rank-nullity theorem allow us to determine the rank of the execution by first determining the rank of every edge map in $\psi_{\rho(i)}$.

Lemma 7. *Let $i < |\Lambda| - 1$. For every edge $e = (\rho(i), \rho(i+1))$, the rank of the edge map $\psi_e : V^i \to V^{i+1}$ is bounded from below by*

$$\mathrm{rank}(\psi_e) \geq \mathrm{rank}(R_e) - 1.$$

However, if $R_e(G_e)$ is transverse to $f_{\mathrm{tar}(e)}$ then

$$\mathrm{rank}(\psi_e) = \mathrm{rank}(R_e).$$

Proof. To see that $\mathrm{rank}(R_e)$ is bounded from below, realize that $D\phi_\tau^{\mathrm{tar}(e)}$ and DR_e can be expressed in coordinates as $\dim(D_{\mathrm{tar}(e)}) - 1 \times \dim(D_{\mathrm{tar}(e)})$ and $\dim(D_{\mathrm{tar}(e)}) \times \dim(D_{\mathrm{sor}(e)}) - 1$ matrices. Moreover, since $\mathrm{rank}(\phi_\tau^{\mathrm{tar}(e)}) = \dim(D_{\mathrm{tar}(e)}) - 1$ by Theorem 3, it follows from (13) that

$$\begin{aligned} \mathrm{rank}(\psi_e) &\geq \mathrm{rank}(R_e) + \mathrm{rank}(\phi_\tau^{\mathrm{tar}(e)}) - \dim(D_{\mathrm{tar}(e)}) \\ &\geq \mathrm{rank}(R_e) - 1 \end{aligned}$$

as desired.

To show that transversality of $R_e(G_e)$ always implies $\mathrm{rank}(R_e) = \mathrm{rank}(\psi_e)$ we apply the rank-nullity theorem and Lemma 6 to $D\psi_e$, yielding

$$\begin{aligned} \mathrm{rank}(D\psi_e) &= \mathrm{rank}(D\phi_\tau^{\mathrm{tar}(e)} \circ DR_e) \\ &= \mathrm{rank}(DR_e) + \mathrm{nty}(DR_e) - \mathrm{nty}(D\phi_\tau^{\mathrm{tar}(e)} \circ DR_e) \\ &= \mathrm{rank}(DR_e) - \dim(\mathrm{ns}(D\phi_\tau^{\mathrm{tar}(e)}) \cap \mathrm{im}(DR_e)). \end{aligned}$$

Recall from Section 2, equation (6) of Theorem 3 that

$$\mathrm{ns}(D\phi_\tau^{\mathrm{tar}(e)}) = \mathrm{span}\{f_{\mathrm{tar}(e)}\},$$

and that $R_e(G_e)$ transverse to $f_{\mathrm{tar}(e)}$ by definition implies $f_{\mathrm{tar}(e)}(y) \notin \mathrm{im}(DR_e)$ for all $y \in R_e(G_e)$. Then

$$\mathrm{span}\{f_{\mathrm{tar}(e)}\} \cap \mathrm{im}(DR_e) = \emptyset$$

and so $\mathrm{rank}(D\psi_e) = \mathrm{rank}(DR_e)$. Noting that $\mathrm{rank}(D\psi_e) = \mathrm{rank}(\psi_e)$ and $\mathrm{rank}(DR_e) = \mathrm{rank}(R_e)$ yields our desired result. □

Remark 5. Lemma 7 implies that the rank of an edge map is only known exactly when the transversality of $R_e(G_e)$ is guaranteed, regardless of whether $\dim(D_{\mathrm{tar}(e)})$ is greater than or less than $\dim(D_{\mathrm{sor}(e)})$. Since we cannot determine the rank of all edge maps where transversality is not guaranteed, we cannot determine the exact rank of the execution.

Thus, in order to obtain a tighter lower bound on the rank of the execution, we must keep track of the number of edges where $R_e(G_e)$ may not be transverse to $f_{\mathrm{tar}(e)}$. Because we only assume that we have transversality (**A4**) when $\dim(D_{\mathrm{sor}(e)}) \leq \dim(D_{\mathrm{tar}(e)})$, we need only keep track of the number of domains that have source domains that are greater in dimension than their target domains.

The following definitions allow us to track the progress of the execution through the graph Γ of $\mathcal{H}$.

Definition 6. Given $i < |\Lambda| - 1$, the set of *traversed edges* is

$$E_i = \{e_{\rho(0)}, \ldots, e_{\rho(i-1)}\},$$

and the set of *visited vertices* is the set of all source and target vertices of E_i,

$$Q_i = \mathrm{sor}(E_i) \cup \mathrm{tar}(E_i) = \{\rho(0), \ldots, \rho(i)\}.$$

Definition 7. Let m be the number of *non-transverse edges* for which we do not assume $R_e(G_e)$ is transverse to $f_{\mathrm{tar}(e)}$. Then m is given by

$$m = \left|\{e \in E_i : \dim(D_{\mathrm{sor}(e)}) > \dim(D_{\mathrm{tar}(e)})\}\right|.$$

We now show that the rank of an execution falls between possibly distinct upper and lower bounds. The following result is the extension of Theorem 4 in [14] to arbitrary, non-periodic hybrid systems and executions.

Theorem 8. *Let $\mathcal{H}$ be a hybrid system with execution χ satisfying assumptions (**A1-4**). For any $i < |\Lambda| - 1$,*

$$\operatorname{rank}(\psi_{\rho(i)}) \leq \min_{e \in E_i}\{\operatorname{rank}(R_e)\} \leq \min_{q \in Q_i}\{\dim(D_q) - 1\},$$

and

$$\operatorname{rank}(\psi_{\rho(i)}) \geq \sum_{e \in E_i} \operatorname{rank}(R_e) - m - \sum_{q \in \operatorname{sor}(E_i) - \{\rho(0)\}} (\dim(D_q) - 1)$$

where m, E_i and Q_i are given in Definitions 6 and 7.

Proof. We show first that the rank of $D\psi_{\rho(i)}$ is bounded from above by the smallest-rank reset map. Since, for any $e \in E$, the derivative of the edge map is $D\psi_e = D\phi_\tau^{\operatorname{tar}(e)} \circ DR_e$, and $\operatorname{rank}(D\phi_\tau^{\operatorname{tar}(e)}) = \dim(D_{\operatorname{tar}(e)}) - 1$ by Theorem 3, equation (12) implies that

$$\operatorname{rank}(D\psi_e) \leq \min\{\operatorname{rank}(DR_e), \dim(D_{\operatorname{tar}(e)}) - 1\}.$$

Applying (12) again, to equation (11), yields

$$\begin{aligned} \operatorname{rank}(D\psi_{\rho(i)}) &= \operatorname{rank}(D\psi_{e_{\rho(i-1)}} \circ \cdots \circ D\psi_{e_{\rho(0)}}) \\ &\leq \min_{e \in E_i}\{\operatorname{rank}(D\psi_e)\}. \end{aligned}$$

It follows that

$$\operatorname{rank}(D\psi_{\rho(i)}) \leq \min\Big\{ \min_{e \in E_i}\{\operatorname{rank}(R_e)\}, \min_{q \in Q_i}\{\dim(D_q) - 1\}\Big\}.$$

Finally, because $\operatorname{rank}(R_e) \leq \dim(D_{\operatorname{sor}(e)}) - 1$,

$$\min_{e \in E_i}\{\operatorname{rank}(R_e)\} \leq \min_{q \in Q_i}\{\dim(D_q) - 1\},$$

which yields the upper bound on $\operatorname{rank}(D\psi_{\rho(i)}) = \operatorname{rank}(\psi_{\rho(i)})$.

We obtain the lower bound on $D\psi_{\rho(i)}$ by applying equation (13) and Lemma 7 to (11). Note that, as stated in the proof of Lemma 7, the derivative $D\psi_e$ of every edge

map can be expressed in coordinates as a $\dim(D_{\mathrm{tar}(e)}) - 1 \times \dim(D_{\mathrm{sor}(e)}) - 1$ matrix. Applying equation (13), we obtain[3]

$$\operatorname{rank}(D\psi_{\rho(i)}) \geq \sum_{e \in E_i} \operatorname{rank}(D\psi_e) - \sum_{q \in \mathrm{sor}(E_i) - \{\rho(0)\}} (\dim(D_q) - 1)\,.$$

Since — by assumption (**A4**) and Definition 7 — there are exactly m edges in E_i where transversality in the target domain is not guaranteed, applying Lemma 7 to the above inequality yields the desired lower bound on $\operatorname{rank}(D\psi_{\rho(i)}) = \operatorname{rank}(\psi_{\rho(i)})$. □

Remark 6. Although the rank of each reset map and the dimension of every domain is typically known *a priori*, if the bounds on $\operatorname{rank}(D\psi_{\rho(i)})$ are distinct then we cannot know the exact rank of the execution without first simulating it. On the other hand, if the upper and lower bounds on rank are equal then every execution accepted by $\mathcal{H}$ necessarily has maximal rank at every point.

If the upper and lower bounds on rank in Theorem 8 are distinct then there must be a mechanism that causes an execution to fail to have maximal rank. We determine this mechanism in the next section.

3.3. Rank deficiency of hybrid executions

Our objective is to understand the causes of rank deficiency; this could, for example, enable the design of controllers that improve the stability properties of hybrid systems. As we will see, rank deficiency can result in superstable hybrid systems that are completely insensitive to perturbations in initial conditions. We begin by formally defining the rank deficiency of a hybrid execution.

Definition 8. Let $\mathcal{H}$ be a hybrid system with execution χ satisfying assumptions (**A1-4**). We say the execution is *rank deficient* at a point $c_i(t_{i+1})$, $i < |\Lambda| - 1$, if $\psi_{\rho(i)}(c_i(t_{i+1}))$ does not have maximal rank, that is, if

$$\operatorname{rank}\left(\psi_{\rho(i)}(c_0(t_0))\right) < r,$$

where r is the upper bound on $\operatorname{rank}(\psi_{\rho(i)})$ from Theorem 8.

[3]Note that n_i in equation (13) corresponds to the number of columns of A_i, implying $n_i = \dim(D_{\mathrm{sor}(e)}) - 1$ for each $e \in \mathrm{sor}(E_i) - \{\rho(i)\}$.

The following Theorem is the main result of this paper. It identifies the intersection of particular tangent spaces over the execution as the primary mechanism causing an execution to fail to have maximal rank. We will address the significance of this result to the potential design of stability-improving controllers both after its proof and throughout the remainder of the paper.

Theorem 9. *Let $\mathcal{H}$ be a hybrid system with execution χ satisfying* (**A1-4**)*, initial condition $x_0 = c_0(t_0)$ and $i < |\Lambda| - 1$. Then $\psi_{\rho(i)}$ is rank deficient if and only if*

$$\sum_{e \in E_i - \{e_{\rho(0)}\}} \dim(\mathrm{ns}(D\psi_e) \cap \mathrm{im}(D\psi_{\mathrm{sor}(e)})) > \mathrm{rank}(\psi_{e_{\rho(0)}}) - r,$$

where r is the upper bound on $\psi_{\rho(i)}$ from Theorem 8.

Proof. The proof will follow from recursively applying the rank-nullity theorem and Lemma 6 to the sequence of linear maps (11).

First, realize that any two linear maps defined on the same domain are related by the rank-nullity theorem. In particular, it is an immediate consequence of rank-nullity that for all j such that $i \geq j \geq 2$,

$$\begin{aligned} \dim(T_{c_0(t_0)}V^0) &= \mathrm{rank}(D\psi_{e_{\rho(0)}}) + \mathrm{nty}(D\psi_{e_{\rho(0)}}) \\ &= \mathrm{rank}(D\psi_{\rho(j)}) + \mathrm{nty}(D\psi_{\rho(j)}), \end{aligned}$$

where the statement is obvious for $j = 1$ since $\psi_{\rho(1)} = \phi_\tau^{\rho(1)} \circ R_{e_{\rho(0)}} = \psi_{e_{\rho(0)}}$. Thus, the rank-nullity of $\psi_{\rho(i)}$ is certainly equal to the rank-nullity of $\psi_{\rho(i-1)}$:

$$\mathrm{rank}(D\psi_{\rho(i)}) + \mathrm{nty}(D\psi_{\rho(i)}) = \mathrm{rank}(D\psi_{\rho(i-1)}) + \mathrm{nty}(D\psi_{\rho(i-1)}).$$

Applying Lemma 6 to the above equation while noting that $\psi_{\rho(i)} = \psi_{e_{\rho(i-1)}} \circ \psi_{\rho(i-1)}$ yields

$$\mathrm{rank}(D\psi_{\rho(i)}) = \mathrm{rank}(D\psi_{\rho(i-1)}) - \dim(\mathrm{ns}(D\psi_{e_{\rho(i-1)}}) \cap \mathrm{im}(D\psi_{\rho(i-1)})).$$

If we continue in this vein by relating the rank-nullity of $\psi_{\rho(j)}$ with $\psi_{\rho(j-1)}$ for $j = i-1, \ldots, 2$, we obtain

$$\mathrm{rank}(D\psi_{\rho(i)}) = \mathrm{rank}(D\psi_{e_{\rho(0)}}) - \sum_{e \in E_i - \{e_{\rho(0)}\}} \dim(\mathrm{ns}(D\psi_e) \cap \mathrm{im}(D\psi_{\mathrm{sor}(e)})). \tag{14}$$

The result follows by observing that $\text{rank}(D\psi_{\rho(i)}) = \text{rank}(\psi_{\rho(i)})$ for all i and that the execution is rank deficient if and only if $r - \text{rank}(\psi_{\rho(i)}) > 0$, where r is the upper bound on rank from Theorem 8. □

Remark 7. The left-hand side of the inequality in the statement of Theorem 9 shows that rank deficiency is primarily affected by the intersection of the nullspace of every reset map with the tangent space over the execution. To see this, realize that for any given $e \in E$, the nullspace of the edge map ψ_e is the union of the tangent spaces

$$\text{ns}(D\psi_e) = \left(\text{ns}(D\phi_\tau^{\text{tar}(e)}) \cap \text{im}(DR_e)\right) \cup \text{ns}(DR_e).$$

Therefore, because the nullspace of the flow to the guard on the target is small, *i.e.*,

$$\text{nty}(D\phi_\tau^{\text{tar}(e)}) = \dim(\text{span}\{f_{\text{tar}(e)}\}) = 1,$$

the nullspace of every edge map is primarily determined by $\text{ns}(DR_e)$. Seen another way, a controller that maximizes the sum

$$\sum_{e \in E_i - \{e_{\rho(0)}\}} \dim(\text{ns}(DR_e) \cap \text{im}(D\psi_{\text{sor}(e)}))$$

for a given execution would be most effective at reducing the rank of that execution.

Remark 8. The right-hand side of Theorem 9 shows that the rank of the first edge map in the execution significantly affects rank deficiency. Since the upper bound on the rank of the execution is $r = \min_{e \in E_i}\{\text{rank}(R_e)\}$, if the initial condition of the execution lies in a domain where $\text{rank}(\psi_{e_{\rho(0)}}) \geq r$, then the execution will not be rank deficient unless enough intersections occur — or the intersections are large enough — so that the inequality of Theorem 9 is satisfied. This can be understood as a consequence of the fact that perturbations to initial conditions will propagate differently through the execution depending on the domain in which it starts.

If the reset map is known exactly then it is easy to compute $\text{ns}(DR_e)$. However, computing $\text{im}(D\psi_{\text{sor}(e)})$ is the same as computing a basis for the linearization of the execution. If an expression for the flow is known in closed form then computing $\text{im}(D\psi_{\text{sor}(e)})$ would be straightforward, because the fundamental matrix solution can be obtained by directly taking partial derivatives of the expression for the flow. But this is not the

case for most systems, and so in general the flow and its fundamental solution must be obtained by simultaneous numerical integration; in most cases it is necessary to simulate the hybrid system in order to check the condition of Theorem 9.

Thus Theorem 9 would make it possible to design controlled, rank deficient hybrid systems through an iterative process involving simulation, confirmation of the conditions of the Theorem, followed by re-design. This type of design flow might be well-suited for use in a dynamic program [25], for example, where the objective of the program would be to maximize the alignment of the tangent spaces over the execution.

In the next Section we discuss how to apply the above results to improve the stability properties of periodic hybrid systems, through an artifact of rank deficiency called *superstability*.

4. Application to Periodic Hybrid Systems

We are interested in applying the general results obtained thus far to periodic solutions of hybrid systems. To this end, we restrict our attention to hybrid systems with cyclic graphs and consider the rank properties of hybrid periodic orbits. We ultimately show that the rank of a periodic orbit is intimately related to the stability of that orbit.

Definition 9. A *hybrid system on a cycle* is a hybrid system $\mathcal{H} = (\Gamma, D, G, R, F)$ where $\Gamma = (Q, E)$ is a *directed cycle* such that $Q = \{q_1, \ldots, q_k\}$ is a set of k vertices and $E = \{e_1 = (q_1, q_2), e_2 = (q_2, q_3), \ldots, e_k = (q_k, q_1)\} \subset Q \times Q$.

Definition 10. A *hybrid periodic orbit* $\mathcal{O} = (\Lambda, I, \rho, C)$ with period T is an execution of the hybrid system on a cycle $\mathcal{H}$ such that for all $n \in \Lambda$,

- $\rho(n) = \rho(n + k)$,
- $I_n + T = I_{n+k}$,
- $c_n(t) = c_{n+k}(t + T)$.

Remark 9. Since $\mathcal{O}$ is periodic we may index the elements S_0^n, S^n, U_0^n, V_0^n and V^n defined in (**H1-2**) using the vertex set Q of the graph Γ of $\mathcal{H}$ rather than the indexing set Λ (for example, one can take $S^n = S^{n+k}$).

Remark 10. As in Remark 3, we do not consider trivial hybrid systems on a cycle, so that $\mathcal{O}$ is never equivalent to the closed periodic orbit of a smooth dynamical system. Thus, Theorem 5 does not apply (see the Remark immediately following the Theorem). The interested reader may wish to consult the authors' work in [14], where the contrast between closed orbits and hybrid periodic orbits is addressed in more detail.

Definition 11. The *fundamental hybrid periodic orbit* associated with $\mathcal{O}$ is the fundamental execution $\mathcal{FO} = (\Lambda, I, \rho, C, W)$, with the fundamental matrix solutions $\Phi_n \in W$ subject to

$$\Phi_n(t - t_n) = \Phi_{n+k}(t + T - t_{n+k}).$$

As previously mentioned, we will not explicitly use the fundamental orbit to state our results on periodic stability.

Extending equations (7) and (10) to periodic orbits yields the following definition for a Poincaré map of a hybrid system.

Definition 12. Let $\mathcal{O}$ be a given hybrid periodic orbit of $\mathcal{H}$ with initial condition $x^* = c_0(t_0) \in D_{\rho(0)}$, where $\rho(0) = q = \rho(k)$ and so $c_0(t_0) = \phi_\tau^q(c_k(t_k))$. The *hybrid Poincaré map* $P_q : V^q \to S^q$ is given by

$$\begin{aligned} P_q(x^*) &= \phi_\tau^{\rho(k)} \circ R_{e_{\rho(k-1)}} \circ \cdots \circ \phi_\tau^{\rho(1)} \circ R_{e_q}(x_0) \\ &= \psi_{e_{\rho(k-1)}} \circ \cdots \circ \psi_{e_q} = \psi_{\rho(k)}. \end{aligned} \tag{15}$$

It is well-known that the stability of hybrid periodic orbits is related to the stability of the hybrid Poincaré map. In particular, the following result is a corollary to Theorem 1 of [26] and the results of [14].

Corollary 10. *Let $\mathcal{H}$ be a hybrid system with hybrid periodic orbit $\mathcal{O}$ satisfying* (**A1-4**)*. Then $x^* = P_q(x^*)$ is an exponentially stable fixed point of the hybrid Poincaré map $P_q : V^q \to S^q$ if and only if $\mathcal{O}$ is exponentially stable.*

As a discrete dynamical system, the stability of the Poincaré map is determined by the eigenvalues of its derivative evaluated at a fixed point. The following is a corollary to Theorem 8.

Corollary 11. *The hybrid Poincaré map $P_q : V^q \to S^q$ is exponentially stable if and only if all eigenvalues of $DP_q(x^*)$ fall within the unit circle. In particular, $P_q(x^*)$ has only $r_q = \text{rank}(DP_q(x^*))$ many nontrivial eigenvalues, where*

$$r_q \leq \min_{e \in E}\{\text{rank}(R_e)\} \leq \min_{q \in Q}\{\dim(D_q) - 1\},$$
$$r_q \geq \sum_{e \in E} \text{rank}(R_e) - m - \sum_{q \in \text{sor}(E) - \{q\}} (\dim(D_q) - 1)\,,$$

m is the number of non-transverse edges in the cycle, and E and Q are the edge and vertex sets of Γ.

It follows that the stability of a rank deficient Poincaré map is determined by fewer eigenvalues than a Poincaré map with maximal rank. However, this does not imply, in general, that rank deficient orbits are more stable than orbits with maximal rank. To assert otherwise would be akin to claiming that lower-dimensional dynamical systems are more stable than higher-dimensional dynamical systems, which is certainly not true in general.

On the other hand, there is a specific case where rank deficiency improves the stability properties of the Poincaré map. Recall that in the context of standard theory [15] a superstable discrete dynamical system is characterized by the derivative of the system equal to 0. When this occurs, the discrete dynamical system is said to be completely insensitive to perturbations in initial conditions. We adapt this notion of superstability to periodic hybrid systems as follows.

Definition 13. The hybrid periodic orbit $\mathcal{O}$ satisfying (**A1-4**) with initial condition x^*, and its associated Poincaré map P_q are said to be *superstable* at x^* if $\text{rank}(DP_q(x^*)) = 0$.

All eigenvalues of a superstable Poincaré map are equal to 0, implying that not only is it exponentially stable, it is completely insensitive to perturbations in initial conditions. We obtain the following Corollary to Theorem 9.

Corollary 12. *The Poincaré map P_q is superstable if and only if the lower bound on rank in Corollary 11 is not greater than* 0 *and*

$$\sum_{e \in E - \{e_q\}} \dim(\text{ns}(D\psi_e) \cap \text{im}(D\psi_{\text{sor}(e)})) = \text{rank}(\psi_{e_q}).$$

Proof. The result follows from equation (14) in the proof of Theorem 9. Noting that $q = \rho(0)$ and that $P_q = \psi_{\rho(k)}$ for a k-domain hybrid system on a cycle, equation (15), we obtain from (14) that

$$\operatorname{rank}(P_q) = \operatorname{rank}(\psi_{\rho(k)}) = \operatorname{rank}(\psi_{e_q}) - \sum_{e \in E - \{e_q\}} \dim(\operatorname{ns}(D\psi_e) \cap \operatorname{im}(D\psi_{\operatorname{sor}(e)})).$$

Recall that P_q is superstable by definition if and only if $\operatorname{rank}(P_q) = 0$. Observing that this is possible if the lower bound on the rank of P_q is equal to 0 yields the desired result. □

Application of the above Corollary and Theorem 9 to single-domain hybrid systems is instructive; we find that periodic single-domain systems are never rank deficient and superstability is determined solely by the discrete transition.

Corollary 13. *Let $\mathcal{H}$ be a single-domain hybrid system on a cycle, that is, let $Q = \{q\}$ and $E = \{e = (q, q)\}$. Then, P_q is never rank deficient and is superstable if and only if*

$$\operatorname{rank}(R_e) = 0.$$

Proof. The Poincaré map of a single-domain system can be written

$$P_q = \psi_{\rho(1)} = \psi_{e_{\rho(0)}} = \phi_\tau^q \circ R_e.$$

From Lemma 7 and assumption (**A4**) we know that $\operatorname{rank}(P_q) = \operatorname{rank}(R_e)$, which is constant by (**A2**). Therefore, since Corollary 11 establishes that the upper bound r on the rank of P_q is

$$r = \min_{e \in E} \{\operatorname{rank}(R_e)\} = \operatorname{rank}(R_e) = \operatorname{rank}(P_q),$$

we see that the Poincaré map of a single-domain hybrid system is by definition never rank deficient. Finally, note that $\operatorname{rank}(P_q) = \operatorname{rank}(R_e) = 0$ if and only if it is superstable. □

The planar compass biped, which we study in Section 4.2, is a periodic single-domain hybrid system. We illustrate our results and the remarks following Theorem 9 on a simple two-domain hybrid system before considering the compass biped.

4.1. Superstability

The following application is a two-domain hybrid system on a cycle $\mathcal{H} = (\Gamma, D, G, R, F)$, with graph structure

$$\Gamma = \big\{Q = \{1, 2\}, E = \{e_1 = (1, 2), e_2 = (2, 1)\}\big\},$$

and domains $D = \{D_1, D_2\}$. We will show that this system is insensitive to perturbations to initial conditions in only one domain.

We define the first domain, D_1, of this system to be the upper-right quadrant of $\mathbb{R}^2$. The vector field on D_1 is

$$f_1(x, y) = \big(-y + x(1 - x^2 - y^2),\, x + y(1 - x^2 - y^2)\big)^T.$$

The flow in this domain is mapped to the next domain, D_2, when it reaches the positive y-axis, which is the guard on D_1: $G_{e_1} = \{x = 0\}$. The reset map R_{e_1} is defined by the immersion of the xy-plane into $\mathbb{R}^3$, $R_{e_1}(x, y) = (x, y, 0)^T$, which has rank 1 on G_{e_1}. As an immersion, $\mathrm{nty}(DR_{e_1}) = 0$.

The second domain is the subset of $\mathbb{R}^3$ defined by $D_2 = \{x \geq 0, y \geq 0, z \geq 0\}$, with linear vector field

$$f_2(x, y, z)^T = (-x, -z, y)^T,$$

and guard $G_{e_2} = \{y = 0\}$. The flow of f_2 is allowed to evolve in D_2 until it reaches the xz-plane, when it is mapped back to the positive x-axis in D_1 by $R_{e_2}(x, y, z) = (x+1, y)^T$, which has rank 1 and nullspace $\mathrm{ns}(DR_{e_2}) = \mathrm{span}\{(0, 0, 1)^T\}$.

This system has a hybrid periodic orbit $\mathcal{O}$ with an initial condition $c_0(t_0) = (1, 0)^T$ in D_1. Define the Poincaré map for initial conditions on the x-axis of D_1, $P_1 : V^1 \to S^1_0$ by

$$P_1 = R_{e_2} \circ \phi^2_\tau \circ R_{e_1} \circ \phi^1_\tau$$

and the Poincaré map for the second domain, $P_2 : V^2 \to S^2_0$ by

$$P_2 = R_{e_1} \circ \phi^1_\tau \circ R_{e_2} \circ \phi^2_\tau,$$

where V^2 is the positive y axis of D_2. It is easy to see that R_{e_1} is transverse to f_2 and R_{e_2} is transverse to f_1; thus the image of both reset maps is transverse to the flow on

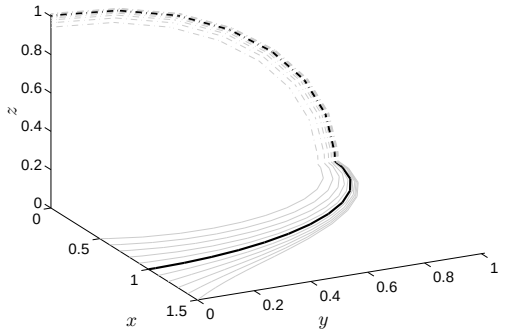

Figure 1: Limit cycle of the superstable two-domain system. The stable cycle is shown in black. The effect of perturbations in the xy-plane (grey) away from the superstable limit cycle (black) are completely removed after one complete traversal of the cycle.

the target domain. With no non-transverse edges, Corollary 11 implies that

$$0 \leq \operatorname{rank}(P_1) \leq 1, \quad \text{and} \quad 0 \leq \operatorname{rank}(P_2) \leq 1.$$

Since the maximum rank of both maps is 1, in this case rank deficiency would also imply superstability.

Applying Theorem 9 directly, we see that in order for P_2 to be rank deficient the following inequality must be true,

$$\dim(\operatorname{ns}(DR_{e_1}) \cap \operatorname{im}\left(D\phi_\tau^1 \circ DR_{e_2} \circ D\phi_\tau^2\right)) > \operatorname{rank}(R_{e_2} \circ \phi_\tau^2) - 1,$$

where the right-hand side evaluates to 0. However, as noted above, DR_{e_1} is an immersion and has no nullspace, so the left-hand side also evaluates to 0 and P_2 cannot possibly be rank deficient. Thus, the inequality is not satisfied because the tangent space over the orbit never aligns with the nullspace of DR_{e_1}.

In order for P_1 to be rank deficient, the inequality

$$\dim\left(\operatorname{ns}(DR_{e_2}) \cap \operatorname{im}\left(D\phi_\tau^2 \circ DR_{e_1} \circ D\phi_\tau^1\right)\right) > 0$$

must be true. Since we can find exact expressions for the flows of both f_1 and f_2, we can compute $D\phi_\tau^1$ and $D\phi_\tau^2$ directly by simply taking partial derivatives. We obtain

$$\operatorname{im}(D\phi_\tau^2 \circ DR_{e_1} \circ D\phi_\tau^1) = \operatorname{span}\{(0,0,1)^T\},$$

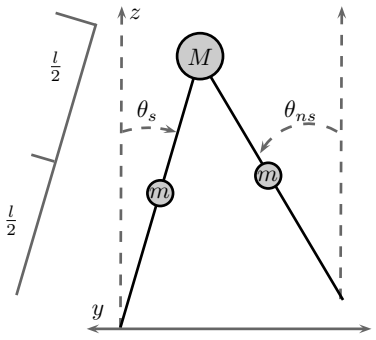

Figure 2: Compass biped dimensions, point-mass locations and measuring conventions.

which, as noted above, is the nullspace of DR_{e_2}. Thus, the nullspace of the reset map aligns with the tangent space over the execution and P_1 is rank deficient. Applying Corollary 12, we confirm that the superstability condition is satisfied for P_1:

$$\dim(\text{span}\{(0,0,1)^T\}) = 1 = \text{rank}(R_{e_1} \circ \phi_\tau^1).$$

This result is easily confirmed through simulation. All trajectories with initial conditions on the x-axis converge to the limit cycle after one iteration of the cycle, as shown in Figure 1.

In this application, the simplicity of the vector fields in each domain allowed us to easily analyze rank deficiency and superstability without numerical integration. Superstability of P_1 was achieved by alignment of the reset map's nullspace with the tangent space over the execution. This could not be achieved for P_2 because R_{e_1} was an immersion; thus, as noted in Remark 8, perturbations to initial conditions will propagate differently through the execution depending on the domain from which they originate.

In the following applications it will be necessary to numerically integrate the fundamental matrix solutions on each domain in order to analyze rank deficiency.

4.2. Planar compass biped

In this section we consider the compass biped, a single-domain periodic hybrid system that has been studied extensively in multiple contexts, with some recent work including [18] and [27]. The objective of this application is to show that the total derivative of the compass biped Poincaré map accurately predicts period-doubling bifurcations.

Period-doubling bifurcations of hybrid systems have been studied extensively in the literature. In [13, 11] the authors derive "jump conditions" and external formula that determine the linearization of the system after a discontinuity. These formula, however, do not apply to multi-domain hybrid systems with domains that are of different dimensions, like the application in the following subsection. In [28] analysis of bifurcations of a certain class of linear relay systems is aided by the fact that straightforward expressions for their Poincaré maps can be found in closed form. The dynamics of bipedal systems, however, are nonlinear and sufficiently complicated as to require numerical integration for complete analysis of either their bifurcation or rank deficiency properties. The equations and analysis described in previous Sections allow for this analysis.

The compass biped is a 2-link planar robotic mechanism capable of walking down a shallow slope without control, see Figure 2. The links form the biped's legs, with the rotary joint connecting them forming its hip. The stance link is assumed fixed to the slope and the nonstance link is free to swing above the slope. The hybrid system model for this simple mechanism is $\mathcal{H} = (\Gamma, D, G, R, F)$ with graph structure $\Gamma = \{Q = \{q\}, E = \{e_q = (q, q)\}\}$. As this is a 2-link mechanism, the dynamics evolve on the tangent bundle to the configuration space $\Theta := \mathbb{T}^2$. We give the dynamics on D_q coordinates $\theta = (\theta_s, \theta_{ns}, \dot{\theta}_s, \dot{\theta}_{ns})^T$, where the angles of the stance and nonstance legs from the vertical are denoted θ_s and θ_{ns}, respectively. We denote the vector field describing the biped dynamics as $\dot{\theta} = f_q(\theta; p)$, where p is the angle of the slope from the horizontal[4]. The guard, G_e, is defined by the holonomic constraint function $h : D_q \to \mathbb{R}$ corresponding to the shallow slope,

$$G_e = \Big\{ h(\theta) = 0 = (\sin(\theta_s) - \sin(\theta_{ns}))\, \tan(p) + (\cos(\theta_s) - \cos(\theta_{ns})) \Big\}.$$

When the nonstance leg impacts the slope we model the jump in link velocities as an instantaneous plastic impact using the reset map $R_e : G_e \to R_e(G_e)$. We refer the reader interested in further modeling details to [29] and [10] for a comprehensive overview.

Let $\mathcal{O}$ be a hybrid periodic orbit for $\mathcal{H}$ with fixed point θ^*. It was first noted in [10] that the compass biped has a period-doubling bifurcation when the angle of the slope is increased to a certain angle. Denote the angle of the slope at the first period-doubling

[4]The notation $f_q(\theta; p)$ indicates that θ is an argument of the function f_q and p is a parameter.

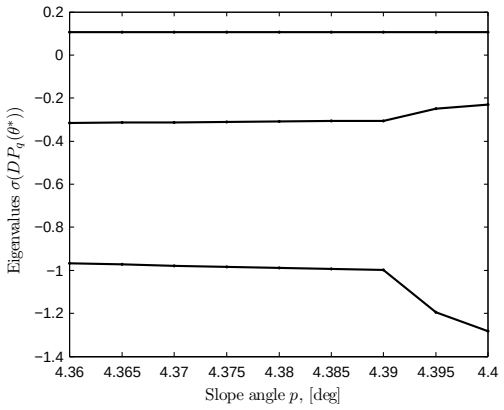

Figure 3: The 3 eigenvalues of $DP_q(\theta^*)$ are plotted versus the angle of incline of the slope. Note that all eigenvalues are within the unit circle except for one, which crosses -1 at $p = 4.39°$.

bifurcation by p^* and define the Poincaré map, $P_q : V^q \to S^q$, as in equation (15). Because $\mathcal{H}$ has only one domain, and R_e has full rank on the guard, applying Corollary 11 implies that

$$\text{rank}(P_q) = \text{rank}(R_e) = 3.$$

We will confirm this by computing the total derivative of P_q,

$$DP_q(\theta^*) = D\phi^q_\tau\left(R_e(\theta^*)\right) DR_e(\theta^*),$$

at the fixed point.

The derivative of the reset map is obtained by simply taking partial derivatives with respect to θ. The total derivative of the flow, $D\phi^q_\tau\left(R_e(\theta^*)\right)$, is obtained using equation (9), where $x_1 = P_q(\theta^*)$, $Dh_j(x_1) = Dh(P_q(\theta^*))$ is the derivative of the holonomic constraint function, and $f_{\rho(j)}(x_1) = f_q(P_q(\theta^*); p^*)$. As noted previously, in order to obtain $\Phi_j(\tau(x^*)) = \Phi_q(\tau(\theta^*))$ it is necessary to integrate $\dot\theta = f_q(\theta; p)$ together with $\dot\Phi_q = Df_q(\theta(t); p)\,\Phi_q(t)$ until the system reaches the guard[5]. Note that the derivative of the vector field is taken with respect to θ, only.

We begin by studying how the eigenvalues of DP_q change as the slope of the ground is increased from $p = 4.36°$ to $p = 4.4°$. Evaluating the derivative of the Poincaré map

[5]The vector fields are simultaneously integrated from initial conditions $R_e(\theta^*)$ and Id_4.

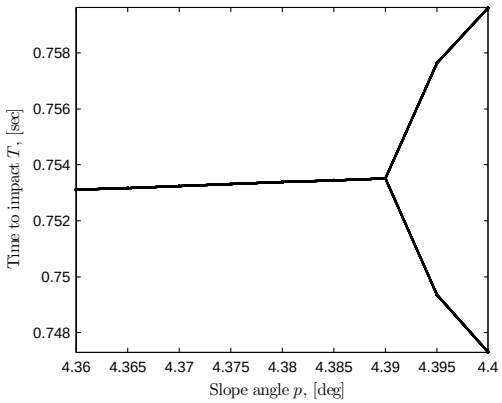

Figure 4: The time it takes the nonstance leg to reach G_e is shown versus p, the angle of incline of the slope. After the slope increases beyond 4.39°, two impacts with the ground are necessary for the biped to complete a single hybrid periodic orbit; the biped "limps" down the slope.

at the fixed point associated with each parameter value yields the bifurcation diagram shown in Figure 3. Note that all eigenvalues are within the unit circle except for one, which crosses -1 at $p = 4.39°$. It is well-known [15] that the linearization of a discrete dynamical system has an eigenvalue equal to -1 at the period-doubling bifurcation [15]. We confirm that we do indeed have a period-doubling bifurcation from Figure 4, which plots the time T it takes for the swing leg to impact the ground over several steps; it is clear from the figure that the biped has stable, 2-periodic hybrid orbits for slopes greater than 4.39°. We have therefore confirmed that the eigenvalues of $DP_q(\theta^*)$ correctly reflect that we have a bifurcation at $\phi^* = 4.39°$. The fixed point corresponding to this parameter value is

$$\theta^* = (0.385171, -0.231931, 1.729380, 2.183038)^T,$$

measured in radians and radians per second, and the eigenvalues of the Poincaré map are

$$\sigma(DP_q(\theta^*)) = (-0.999085, 0.105681, 1.384626\text{E-}15, -0.305354).$$

Note that one eigenvalue is nearly within machine precision of 0, so the rank of the Poincaré map is equal to 3, as predicted by Corollary 11.

Figure 5 shows the phase portrait of the system for values of ϕ just before and just after bifurcation. After passing the bifurcation point, the compass biped needs to take

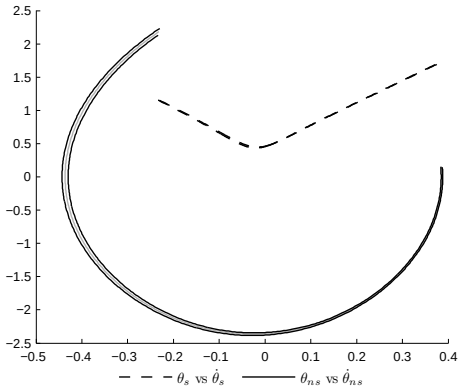

Figure 5: The phase portrait corresponding to two steps of the compass biped, for slope values just before ($p^* = 4.385$ shown in gray) and just after bifurcation ($p^* = 4.395$ shown in black). The "limping" behavior is apparent in the non-stance leg (shown solid) after passing the bifurcation point

two full steps in order to complete a cycle; the biped shows a slight "limping" behavior after passing the period-doubling bifurcation. This behavior is evident in the phase portrait, which shows two separate solid black lines corresponding to the movement of the swing leg. One line indicates a faster leg swing and the other a slower swing, compared to the swing leg movement just before bifurcation shown in solid gray.

In Corollary 13 we showed that periodic single-domain hybrid systems are never rank deficient and are superstable if only if the reset map has constant rank equal to 0. The following application extends the compass biped to a two-domain system that is possibly rank deficient, and superstable in only one of its two domains.

4.3. Planar kneed biped

Our second application to periodic systems is a controlled planar biped with locking knees walking on flat ground, as studied in [30]. It may be considered the augmentation of the planar compass biped with an additional domain where the stance leg is locked and the non-stance leg is unlocked at the knee. See Figure 6.

We model the planar kneed biped as a two-domain hybrid system on a cycle $\mathcal{H} = (\Gamma, D, G, R, FG)$ with graph structure

$$\Gamma = \big\{Q = \{u, l\}, E = \{e_u = (u, l), e_l = (l, u)\}\big\}.$$

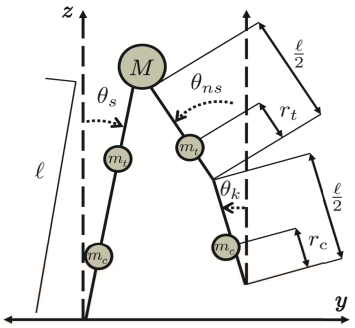

Figure 6: Diagram of a planar kneed biped. The annotations indicate dimensions, point-mass locations and measuring conventions for stance, calf and thigh angles from the vertical.

In the *unlocked domain* D_u, the non-stance calf rotates about the knee and we model the biped as a 3-link planar mechanism. The dynamics evolve on the tangent bundle to the configuration space $\Theta_u := \mathbb{T}^3$, which we give coordinates $\theta_u = (\theta_s, \theta_{ns}, \theta_k)^T$ with the stance leg angle denoted by θ_s, non-stance thigh angle by θ_{ns}, and non-stance calf angle by θ_k. Each angle is measured from the vertical. Since the non-stance thigh and calf are locked together in the *locked domain* D_l, the biped is modeled as a 2-link mechanism, so the dynamics evolve on the tangent bundle to the configuration space $\Theta_l := \mathbb{T}^2$ with coordinates $\theta_l = (\theta_s, \theta_{ns})^T$. We transition from D_u to D_l when the knee locks, and from D_l to D_u when the foot strikes the ground.

The reset maps $R = \{R_{e_u}, R_{e_l}\}$ model transitions between the locked and unlocked domains. We make the standard assumption that all impacts are perfectly plastic; detailed discussions of and formulas for the impact map may be found in [18, 31, 30] and so will not be repeated here. However, it is worth noting that since $\dim(D_u) = 4$ and $\dim(D_l) = 6$, $\dim(\mathrm{ns}(DR_{e_l})) = 2$ since it maps to a lower-dimensional domain. On the other hand, DR_{e_u} does not have a nullspace, since it maps to a larger-dimensional domain.

Finally, since we want the kneed biped to walk on flat ground, we use controlled symmetries [32, 30] for our controlled vector fields $FG = \{f_u, f_l\}$ on each domain.

Define the Poincaré map for initial conditions in the locked domain by

$$P_l = \phi_\tau^l \circ R_{e_u} \circ \phi_\tau^u \circ R_{e_l},$$

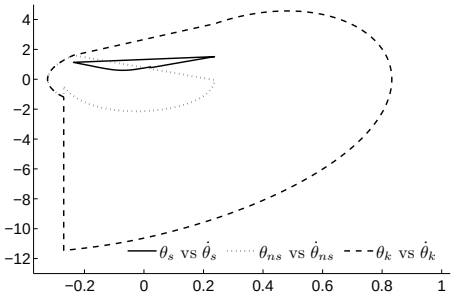

Figure 7: Planar kneed biped phase portrait. In D_l the non-stance calf angle θ_k (shown dashed) is equal to the non-stance angle θ_{ns} (dashed-dotted).

and in the unlocked domain by

$$P_u = \phi_\tau^u \circ R_{e_l} \circ \phi_\tau^l \circ R_{e_u}.$$

Applying Corollary 11, we find that

$$2 \leq \text{rank}(P_u) \leq 3, \quad \text{and} \quad 0 \leq \text{rank}(P_l) \leq 3,$$

so that the stability of the planar kneed biped is determined by at most 3 eigenvalues; this has been numerically confirmed in [14]. Since the lower bound on P_l is equal to 0, it may be possible to use a combination of finite-time controllers on the dynamics in D_l and D_u to align the tangent space over the orbit with the 2-dimensional nullspace of DR_{e_l}, making the biped completely rank deficient, and thus insensitive to perturbations in D_l. On the other hand, perturbations in D_u cannot be completely canceled in D_u, since $\text{rank}(P_u) \geq 2$.

It is impossible to confirm Corollary 12 without first simulating the system. We numerically compute that DP_u and DP_l both have three stable eigenvalues [14]. Simulating the system from the fixed point

$$c_0(t_0) = c_0(t_1) = (0.021462,\, -0.26990,\, -0.26990, 0.82882,\, -0.45645,\, -11.454)^T$$

with slope $p = \pi/60$ (see Figure 7) allows us to verify that $\mathcal{O}$ does not satisfy the condition of Corollary 12, that is, $\text{ns}(DR_{e_l})$ does not align with the tangent space over $\mathcal{O}$. Thus, this particular orbit of the planar kneed biped with controlled symmetries has maximal rank.

5. Conclusion

We have shown that the rank of a hybrid execution is always less than the dimension of the space on which solutions evolve. The upper and lower bounds on the rank are known *a priori*. The rank deficiency condition is determined by the alignment of the nullspace of each reset map with the tangent space to the execution. We applied our results to a periodic orbit and observed superstability, which is a desirable artifact of rank deficiency, and noted that the eigenvalues of the linearization of the Poincaré map correctly reflect the occurrence of period-doubling behavior in a compass biped.

The results presented in this paper emphasize fundamental differences between smooth and hybrid systems, implying a depth to hybrid systems that is not yet fully understood. We have shown that these differences result in behavior in hybrid systems that cannot be obtained in smooth systems. In particular, as an application of the rank deficiency conditions we derived, we considered the superstability of periodic orbits of hybrid systems, a type of stability not found in continuous dynamical systems. A very interesting future research direction is to create techniques that take advantage of existing geometric tools — such as those used in [33] — that allow for the design of controllers that directly exploit the rank properties of hybrid systems so as to achieve superstability. This will imbue the resulting controlled hybrid system with an increased resistance to perturbations and hence greater robustness.

Acknowledgments

We thank the reviewers for their many valuable comments, corrections and suggestions.

References

[1] A. Bayen, P. Grieder, H. Sipma, G. Meyer, C. Tomlin, Delay predictive models of the national airspace system using hybrid control theory, in: American Control Conference, 2002. Proceedings of the 2002, Vol. 1, 2002, pp. 767 – 772 vol.1. doi:10.1109/ACC.2002.1024907.

[2] C. Tomlin, J. Lygeros, S. Shankar Sastry, A game theoretic approach to controller design for hybrid systems, Proceedings of the IEEE 88 (7) (2000) 949 –970. doi:10.1109/5.871303.

[3] J. Lygeros, K. Johansson, S. Simic, J. Zhang, S. Sastry, Continuity and invariance in hybrid automata, in: Decision and Control, 2001. Proceedings of the 40th IEEE Conference on, Vol. 1, 2001, pp. 340 –345 vol.1. doi:10.1109/.2001.980123.

[4] Y. Hurmuzlu, F. Gnot, B. Brogliato, Modeling, stability and control of biped robots–a general framework, Automatica 40 (10) (2004) 1647 – 1664. doi:DOI: 10.1016/j.automatica.2004.01.031.

[5] M. Broucke, Regularity of solutions and homotopic equivalence for hybrid systems, in: Decision and Control, 1998. Proceedings of the 37th IEEE Conference on, Vol. 4, 1998, pp. 4283 –4288 vol.4. doi:10.1109/CDC.1998.761978.

[6] J. Lygeros, K. Johansson, S. Sastry, M. Egerstedt, On the existence of executions of hybrid automata, in: Decision and Control, 1999. Proceedings of the 38th IEEE Conference on, Vol. 3, 1999, pp. 2249 –2254 vol.3. doi:10.1109/CDC.1999.831255.

[7] J. Lygeros, K. Johansson, S. Simic, J. Zhang, S. Sastry, Dynamical properties of hybrid automata, Automatic Control, IEEE Transactions on 48 (1) (2003) 2 – 17. doi:10.1109/TAC.2002.806650.

[8] G. Davrazos, N. Koussoulas, A review of stability results for switched and hybrid systems, in: Mediterranean Conference on Control and Automation, 2001.

[9] A. Lamperski, A. Ames, Lyapunov-like conditions for the existence of zeno behavior in hybrid and lagrangian hybrid systems, in: Decision and Control, 2007 46th IEEE Conference on, 2007, pp. 115 –120. doi:10.1109/CDC.2007.4435003.

[10] A. Goswami, B. Thuilot, B. Espiau, Compass-like biped robot part i: Stability and bifurcation of passive gaits, Tech. Rep. 2996, INRIA (October 1996).

[11] R. Leine, H. Nijmeijer, Dynamics and bifurcations of non-smooth mechanical systems, Springer Verlag, 2004.

[12] I. Hiskens, Stability of hybrid system limit cycles: Application to the compass gait biped robot, in: IEEE Conference on Decision and Control, Vol. 1, IEEE; 1998, 2001, pp. 774–779.

[13] I. Hiskens, M. Pai, Trajectory sensitivity analysis of hybrid systems, IEEE Transactions on Circuits and Systems I: Fundamental Theory and Applications 47 (2) (2000) 204–220.

[14] E. D. Wendel, A. D. Ames, Rank Properties of Poincaré Maps for Hybrid Systems with Applications to Bipedal Walking, in: HSCC '10: Proceedings of the 13th ACM international conference on Hybrid systems: computation and control, ACM, 2010, pp. 151–160. doi:http://doi.acm.org/10.1145/1755952.1755975.

[15] S. H. Strogatz, Nonlinear dynamics and chaos: with applications to physics, biology, chemistry, and engineering, Westview Press, Cambridge, MA, 2000.

[16] T. McGeer, Passive dynamic walking, The International Journal of Robotics Research 9 (2) (1990) 62–82. arXiv:http://ijr.sagepub.com/content/9/2/62.full.pdf+html, doi:10.1177/027836499000900206.

[17] S. Collins, A. Ruina, A bipedal walking robot with efficient and human-like gait, in: Robotics and Automation, 2005. ICRA 2005. Proceedings of the 2005 IEEE International Conference on, 2005, pp. 1983 – 1988. doi:10.1109/ROBOT.2005.1570404.

[18] J. Grizzle, G. Abba, F. Plestan, Asymptotically stable walking for biped robots: Analysis via

systems with impulse effects, IEEE Transactions on Automatic Control 46 (1) (2001) 51–64.

[19] M. Hirsch, S. Smale, Differential equations, dynamical systems, and linear algebra, Academic Press Inc, 1974.

[20] L. Perko, Differential equations and dynamical systems, Springer, 2001.

[21] T. Parker, L. Chua, Practical numerical algorithms for chaotic systems, Springer-Verlag New York, Inc. New York, NY, USA, 1989.

[22] H. Khalil, Nonlinear systems, Prentice hall Englewood Cliffs, NJ, 1996.

[23] S. Smale, Stable manifolds for differential equations and diffeomorphisms, Ann. Sc. Norm. Super. Pisa, Sci. Fis. Mat., III. Ser. 17 (1963) 97–116.

[24] S. Lang, Introduction to linear algebra, 2nd Edition, Springer-Verlag, New York, 1986.

[25] F. Lewis, V. Syrmos, Optimal control, Wiley-Interscience, 1995.

[26] B. Morris, J. Grizzle, A restricted poincare map for determining exponentially stable periodic orbits in systems with impulse effects: Application to bipedal robots, in: 44th IEEE Conference on Decision and Control, 2005 and 2005 European Control Conference. CDC-ECC'05, 2005, pp. 4199–4206.

[27] D. Pekarek, A. Ames, J. Marsden, Discrete mechanics and optimal control applied to the compass gait biped, in: IEEE Conference on Decision and Control and European Control Conference ECC, New Orleans, USA, 2007.

[28] M. di Bernardo, K. Johansson, F. Vasca, Self-oscillations and sliding in relay feedback systems: Symmetry and bifurcations, International Journal of Bifurcations and Chaos 11 (4) (2001) 1121–1140.

[29] E. R. Westervelt, Feedback Control of Dynamic Bipedal Robot Locomotion, no. 1 in Control and automation, CRC Press, Boca Raton, 2007.

[30] A. Ames, R. Sinnet, E. Wendel, Three-dimensional kneed bipedal walking: A hybrid geometric approach, in: R. Majumdar, P. Tabuada (Eds.), Hybrid Systems: Computation and Control, Vol. 5469 of Lecture Notes in Computer Science, Springer Berlin / Heidelberg, 2009, pp. 16–30.

[31] A. D. Ames, R. D. Gregg, E. D. Wendel, S. Sastry, On the Geometric Reduction of Controlled Three-Dimensional Bipedal Robotic Walkers, in: Proc. 3rd IFAC Workshop on Lagrangian and Hamiltonian Methods for Nonlinear Control, Nagoya, Japan, 2006, pp. 189–202.

[32] M. Spong, F. Bullo, Controlled symmetries and passive walking, IEEE Transactions on Automatic Control 50 (7) (2005) 1025–1031.

[33] D. Tyner, A. Lewis, Jacobian linearisation in a geometric setting, in: Decision and Control, 2003. Proceedings. 42nd IEEE Conference on, Vol. 6, 2003, pp. 6084 – 6089 Vol.6. doi:10.1109/CDC.2003.1272230.